HHS Public Access

Author manuscript

Nat Methods. Author manuscript; available in PMC 2014 February 01.

Published in final edited form as:

Nat Methods. 2013 August ; 10(8): 751–754. doi:10.1038/nmeth.2521.

Near-infrared fluorescent proteins for multicolor *in vivo* imaging

Daria M. Shcherbakova[1,2] and **Vladislav V. Verkhusha**[1,2]

[1]Department of Anatomy and Structural Biology, Albert Einstein College of Medicine, Bronx, NY 10461, USA

[2]Gruss-Lipper Biophotonics Center, Albert Einstein College of Medicine, Bronx, NY 10461, USA

Abstract

Near-infrared fluorescent proteins are in high demand for *in vivo* imaging. We developed four spectrally distinct fluorescent proteins, iRFP670, iRFP682, iRFP702, and iRFP720, from bacterial phytochromes. iRFPs exhibit high brightness in mammalian cells and tissues and are suitable for long-term studies. iRFP670 and iRFP720 enable two-color imaging in living cells and mice using standard approaches. Five iRFPs including previously engineered iRFP713 allow multicolor imaging in living mice with spectral unmixing.

Deep optical imaging in mammalian tissues and whole mammals requires near-infrared (NIR) fluorescent probes. In a so called NIR “optical window” (from 650 nm to 900 nm) the mammalian tissue is more transparent to light because combined absorption of hemoglobin, melanin and water is minimal[1]. In addition, reduced autofluorescence and low light scattering makes this spectral region preferable for deep-tissue imaging.

Efforts to engineer GFP-like fluorescent proteins (FPs) into far-red probes have resulted in several fluorescent FPs shown to be useful in mammals, such as E2-Crimson[2], mNeptune[3], TagRFP657[4], eqFP650[5] and eqFP670[5]. Among them TagRFP657 exhibits the most red-shifted excitation maximum at 611 nm but suffers from low brightness. The photoconverted form of the photoswitchable PSmOrange[6] has an excitation peak at 634 nm, but to appear this form requires photoconversion of the FP with blue light, which poorly penetrates mammalian tissues.

Bacterial phytochrome photoreceptors (BphPs) are promising templates for engineering of NIR FPs[7]. Phytochromes, found in plants, fungi, bacteria, and cyanobacteria, are a superfamily of photoreceptors, which use different types of tetrapyrroles as chromophores.

Correspondence should be addressed to V.V.V. (vladislav.verkhusha@einstein.yu.edu).

AUTHOR CONTRIBUTIONS

D.M.S. developed the proteins and characterized them *in vitro*, in cultured cells, and in mice. V.V.V. directed and planned the project and together with D.M.S. designed the experiments, analyzed the data, and wrote the manuscript.

Note: Supplementary information is available on the Nature Methods website.

COMPETING INTEREST STATEMENT

There are no competing financial interests.

Accession codes. GenBank: KC991142 (iRFP670), KC991143 (iRFP682), KC991144 (iRFP702), and KC991145 (iRFP720).

The subfamily of BphPs is the most attractive source for developing FPs because their absorption spectrum is the most red- shifted among the phytochromes and because they utilize biliverdin IVα (BV) as a chromophore, which is an intermediate of heme metabolism and is ubiquitously found in mammalian tissues[8, 9]. Wild-type BphPs exhibit multidomain architecture, typically consisting of the PAS, GAF, PHY and effector domains. BphPs adopt two spectrally different photochemical states: red absorbing Pr and far-red absorbing Pfr, and more rarely near-red absorbing Pnr[10]. Various BphPs have different absorption maxima in the respective photochemical states[8]. Deletion of the PHY and effector domains from *Deinococcus radiodurans* (*Dr*BphP) and *Rhodopseudomonas palustris* (*Rp*BphP2) BphPs followed by extensive mutagenesis of the PAS and GAF domains resulted in several NIR FPs, namely IFP1.4 (excitation/emission maxima at 684 nm/708 nm)[11], Wi-Phy (excitation/emission maxima at 701 nm/719 nm)[12], and iRFP (excitation/emission maxima at 692 nm/713 nm)[13]. IFP1.4 and iRFP, have been previously utilized for whole-body imaging[11, 13, 14]. IFP1.4 required injection of BV to become fluorescent, but iRFP efficiently incorporated endogenous BV, making its use as easy as conventional GFP-like FPs[13]. iRFP was applied for live imaging of livers[13] and tumors[14] in mice.

Having several spectrally distinct NIR FPs could open new possibilities for labeling two and more tissues and organs, and for tracking several cell populations in a live animal. Here, we report four NIR FPs derived from BphPs, termed iRFP670, iRFP682, iRFP702, and iRFP720 after the maxima of their emission peaks. To avoid confusions, the original iRFP is renamed as iRFP713. A palette of iRFPs enables multicolor NIR imaging *in vivo*.

We started from *Rp*BphP6[8] as a template for further NIR FP engineering. *Rp*BphP6 has an absorbance maximum in the Pr state at 700 nm, 10 nm shorter than a maximum for *Rp*BphP2 (the template for the derivation of iRFP713). First, we cut *Rp*BphP6 to only the PAS and GAF domains, which are required to covalently incorporate BV[15]. Mutations of the invariant key residue D202 and the substitution Y258F (numbering follows that for *Rp*BphP2) were shown to stabilize the chromophore in the Pr state and render the protein fluorescent[12, 16] (Supplementary Fig. 1). We performed saturated mutagenesis of the D202 and adjacent I203 positions. The brightest mutants had the D202V/I203V and D202L/I203V substitutions. After three rounds of random mutagenesis the best mutants were tested for brightness in transiently transfected HeLa cells to eliminate proteins with poor efficiency of folding and incorporation of BV[13]. A final variant, named iRFP702, had excitation and emission maxima at 673 nm and 702 nm, respectively.

We then searched for spectrally shifted variants of iRFP713 and iRFP702 by randomly mutating them and screening the mutants using FACS. As a result, we collected mutants with blue and red shifted spectra in each library. Additionally, key protein positions 180, 202, 203, and 254 were targeted using saturated mutagenesis. After testing spectral properties and effective brightness in HeLa, three final variants were chosen and named iRFP670 (excitation/emission maxima at 643 nm/670 nm), iRFP682 (excitation/emission maxima at 663 nm/682 nm), and iRFP720 (excitation/emission maxima at 702 nm/720 nm) (Table 1 and Fig. 1a,b). Absorbance spectra (Fig. 1c) indicate that all iRFPs efficiently incorporate the BV chromophore, as observed by the presence of peaks at 280 nm and at around 390 nm that correspond to absorbance of BV[13]. To conclude, the molecular

evolution of RpBphP6-PAS-GAF and iRFP713 has resulted in four new NIR FPs with absorbance and fluorescence maxima covering ~50 nm of the respective NIR ranges (Fig. 1d).

Molecular brightness (the product of a molar extinction coefficient and quantum yield) of the new iRFP variants was similar to the brightness of iRFP713 and IFP1.4 (Table 1). Like the templates they are based on[11, 15], the new iRFPs are dimeric and do not contain monomerizing mutations at the C-terminus of their GAF domains[11, 12]. The fluorescence of all iRFPs was stable at pHs between 4 and 8, with p*K*a values of 4.0 for iRFP670 and 4.5 for other iRFPs (Supplementary Fig. 2a). To compare folding and chromophore incorporation kinetics of BphP-based FPs with conventional GFP-like FPs, we monitored fluorescence in bacteria upon pulse-chase induction of protein expression. All BphP-based FPs had half-times for combined folding and chromophore formation comparable to that of EGFP: 4.5-5 h for iRFPs and IFP1.4, and 3 h for EGFP (Supplementary Fig. 2b).

High effective brightness in mammalian cells without addition of exogenous BV is a key advantage of iRFP713 over IFP1.4. We analyzed the effective brightness of newly developed iRFPs in transiently transfected HeLa cells. No external BV was added. The highest fluorescent signal was obtained for iRFP670 (119% of that for iRFP713) and the lowest – for iRFP702 (61%) (Fig. 1e). The effective brightness, which depends on molecular brightness, intracellular stability, affinity for BV, and protein expression level, reveals that the new iRFPs could be as efficient imaging tools as iRFP713.

Epifluorescent microscopy of HeLa cells revealed evenly distributed fluorescence for all iRFPs (Supplementary Fig. 3a). The intracellular photostability of the four iRFPs was lower compared to that of iRFP713 but higher than IFP1.4 (Table 1 and Supplementary Fig. 3b).

We also compared the fluorescent signal of transiently transfected HeLa cells expressing iRFP670 relative to cells expressing the GFP-like far-red FPs E2-Crimson, mNeptune, eqFP650, and eqFP670 (Supplementary Fig. 4). iRFP670 had 6-fold higher mean fluorescence intensities relative to all of these FPs, making it a promising variant for whole cell labeling in applications employing standard red lasers.

To quantitatively compare performance of iRFPs with other far-red FPs for deep-tissue imaging, we used a phantom model engineered to have aufluorescence and light-scattering properties matching those of mouse muscle tissue. Equal amounts of purified FPs were placed inside the phantom at two depths (7.0 mm and 18.1 mm) and imaged in different spectral channels. We quantified the ratios of the fluorescence signal to autofluorescence background and compared the highest values for each FP among different filter channels (Fig. 1f-i). For the most blue-shifted iRFP670, the ratio was 5.6-fold higher at 7.0 mm and 11.7-fold higher at 18.1 mm as compared to mNeptune. For the most red-shifted iRFP720, the ratio was 9.5-fold higher at 7.0 mm and 18.9-fold higher at 18.1 mm than the ratios for mNeptune.

Stability of fluorescence over cell generations correlates with cytotoxicity and is critical for the application of FPs in living animals, especially in long-term studies[17]. To test for this, we compared iRFPs with the least cytotoxic standard EGFP[2] in prolonged expression

conditions. Preclonal mixtures of MTLn3 cells stably expressing FPs were analyzed by FACS 14 days after transfection and subsequently 15 days after the first analysis (Supplementary Fig. 5a). Cells expressing the iRFPs retained more than a half of the signal, with the highest decrease of fluorescence (to 55%) observed in iRFP702-expressing cells and the lowest (to 84%) – in iRFP682-expressing cells (Supplementary Fig. 5b). For comparison, cells expressing EGFP retained 74% of their initial signal. Similar analysis using other mammalian cells resulted in 24% of fluorescence retention for mKate2 and 73% of fluorescence retention for E2-Crimson, the least cytotoxic far-red GFP-like FP[13].

To test the performance of iRFPs in whole-body imaging experiments, we employed a mouse xenograft breast cancer model. MTLn3 cells stably expressing constructs for the different iRFPs were injected into a mammary gland of immunocompromised mice and grown into tumors. The high sensitivity of iRFPs as probes for *in vivo* imaging enabled detection of tumors at early stages (Supplementary Fig. 5c). We monitored the growth of the tumors by epifluorescent whole-body imaging for up to four weeks after cell injection (Supplementary Fig. 6a). Tumors expressing iRFPs produced high NIR fluorescence signal which constantly grew, in contrast to tumors expressing EGFP (Supplementary Fig. 6b). The brightness of the tumors expressing each of the iRFPs correlated with the brightness levels of the different transgenic MTLn3 lines before injection (Supplementary Fig. 6c).

The 50 nm spectral shift between iRFP670 and iRFP720 should allow their use in two-color imaging experiments using a combination of two standard filter channels (excitation/emission maxima at 640 nm/680 nm and 710 nm/760 nm) (Fig. 2a). We quantified the fluorescence signals for each FP in these two filters for bacterial streaks expressing iRFP670 and iRFP720 (or iRFP713) (Supplementary Fig. 7a). The imaging contrast (calculated as the ratio between fluorescence signals of one FP and another FP in the two filter channels) was calculated as 690-fold for the iRFP670/iRFP720 and 510-fold for the iRFP670/iRFP713 pairs.

We then used the iRFPs for two-color imaging in living mice. Two tumors expressing either iRFP670 or iRFP720 were implanted simultaneously into one mouse and grown close to each other, forming the conjoined tumor. The two spatially close fluorescent tissues could be distinguished using two filter channels (excitation/emission maxima at 640 nm/680 nm and 710 nm/760 nm) by whole body imaging (Fig. 2b). The same was true for two tumors of unequal sizes implanted with a time difference of one week (Supplementary Fig. 7b,c).

Next we studied whether two different fluorescent sources could be spectrally separated inside an animal if they are located at different depths. Mice with a mammary gland tumor expressing iRFP670 were infected with adenoviral particles encoding iRFP713, which specifically infect mouse liver. As previously demonstrated[13], fluorescence in the liver was detected starting at the second day after infection. Liver expressing iRFP713 and the closely located tumor expressing iRFP670 could be spectrally separated (Fig. 2c). Using fluorescence imaging tomography we could determine the localization of the two distinct fluorescent tissues in 3D (Supplementary Fig. 8). By *ex vivo* imaging of the isolated tumor and liver tissue, we confirmed iRFP670 and iRFP713 expression in these tissues (Supplementary Fig. 9).

To demonstrate that two-color NIR imaging is also possible in standard epifluorescent microscopy, we imaged HeLa cells co-expressing iRFP670 and either iRFP713 or iRFP720 in two different intracellular organelles: nucleus and mitochondria. A filter setup shown in Figure 2d enabled subcellular imaging of both iRFP670/iRFP720 (Fig. 2e,f) and iRFP670/iRFP713 (Supplementary Fig. 10) pairs in live cells.

A potentially useful application of iRFPs would be simultaneous detection of more than two types of cells, tissues, or transcription activities using spectral imaging techniques. Four types of MTLn3 cells expressing iRFP670, iRFP682, iRFP702, or iRFP720 were detected as separate populations in flow cytometry (Fig. 2g) and with confocal microscopy with spectral detection (Fig. 2h). We next tested how many iRFPs are possible to spectrally unmix *in vivo* using a standard whole-body imaging system with spectral detection, such as IVIS Spectrum. Five types of bacterial cells expressing iRFPs were distinguished using reference spectra for individual streaks (Supplementary Fig. 11). In living mice all five types of tumors also could be unmixed, starting as early as day 12 after the MTLn3 cell injection (Fig. 2i). An *ex vivo* imaging of the isolated tumors confirmed the specificity of the unmixing (Supplementary Fig. 12).

Further studies revealing the chromophore photochemistry responsible for the spectral shifts in iRFPs should allow designing new BphP-based probes with desired spectral properties. This in turn will open the door for engineering of biosensors to noninvasively detect metabolites and enzymatic activities *in vivo*.

Two NIR FPs engineered in this work, iRFP670 and iRFP720, are the most blue- and red-shifted BphP-based fluorescent probes reported to date. All iRFPs have high effective brightness, low cytotoxicity and do not require exogenous BV to fluoresce in mammalian cells and in mice. The multicolor whole-body imaging techniques aided by iRFPs should become common approaches in cell and developmental biology, studies of cancer, pathogen invasion, and biomedicine.

ONLINE METHODS

Mutagenesis and screening of libraries

Internal EcoRI sites were removed from genes encoding both *Rp*BphP6[8] and iRFP proteins[13] using site-specific mutagenesis. A PCR-amplified BglII-EcoRI fragment encoding *Rp*BphP6 PAS-GAF domains (first 310 amino acids) was cloned into the pBAD/His-B vector (Invitrogen). Site-specific mutagenesis was performed using a QuickChange Mutagenesis Kit (Stratagene). For simultaneous mutagenesis at several positions, an overlap-extension approach was applied[18]. Random mutagenesis was performed using a GeneMorph II Random Mutagenesis Kit (Stratagene) or a Diversity PCR Random Mutagenesis Kit (Clontech) under conditions resulting in a mutation frequency of up to 16 mutations per 1,000 base pairs. After mutagenesis, a mixture of mutated genes was electroporated into LMG194 host cells (Invitrogen) containing the pWA23h plasmid facilitating biliverdin synthesis. The pWA23h plasmid contained the rhamnose promoter from the pWA21 plasmid[19], kanamycin resistance, and COLA origin parts from a pCOLADuet-1 plasmid (Novagen). First, the AvrII-PciI fragment containing kanamycin

resistance and COLA origin was PCR amplified from pCOLADuet-1 plasmid and inserted into a pWA21h-AvrIINotI vector. Then, a *hmuO* gene encoding *Bradyrhizobium ORS278* heme oxygenase[20] was PCR amplified from pBAD/HisB-*Rp*BphP2-hmuO plasmid[10] and swapped with a gene encoding EGFP in the pWA21-AvrIINotI plasmid.

Typical mutant libraries consisted of about 10^6-10^8 independent clones. The LMG194 cells were grown overnight at 37°C in RM minimal medium supplemented with ampicillin and kanamycin. Protein expression in the libraries was induced with 0.002% arabinose and 0.02% rhamnose. The cells were grown for 6-8 h at 37°C, then at 18°C for 24 h. Before FACS screening, bacterial cells were washed with phosphate buffered saline (PBS) and diluted with PBS to optical density of 0.03 at 600 nm. The libraries were screened using MoFlo XDP (Beckman Coulter) fluorescence activated cell sorter equipped with argon, krypton and argonkrypton mixed-gas lasers. Typically about 10 sizes of each library were sorted, using a 676 nm laser line for excitation and a 700 nm LP emission filter for positive selection. The brightest collected infra-red bacterial cells were rescued in a SOC medium at 37°C for one hour, and then grown on LB/ampicillin/kanamycin Petri dishes supplemented with 0.02% arabinose, 0.2% rhamnose, 100 μM ALA, and 50 μM $FeCl_3$ overnight at 37°C followed by incubation at 18°C. To search for spectrally shifted libraries of random mutants of iRFP713 and iRFP702 were sorted with combinations of two laser lines (647 nm and 676 nm, in some experiments 592 nm solid state laser was used instead of 647 nm), and emission filters (670/30 nm and 718 nm LP). The dishes were analyzed with Leica MZ16F fluorescence stereomicroscope equipped with equipped with the 650/45 nm excitation and 690 nm LP emission filters (Chroma) and a CCD camera. Screening for spectrally shifted mutants on Petri dishes was performed using IVIS Spectrum instrument (PerkinElmer/Caliper). Approximately 20-50 clones in each screen were selected. Their spectra, and brightness in HeLa cells transfected with plasmids, obtained after swapping with a gene of EGFP in the pEGFP-N1 plasmid (Clontech), were tested, and DNA was sequenced. A mixture of several selected mutants was then used as a template for the next round of mutagenesis.

Protein characterization

The *Rp*BphP6 and iRFP mutants with polyhistidine tags on the N-terminus were expressed in LMG194 bacterial cells grown in RM medium supplemented with ampicillin, kanamycin, 0.002% arabinose, 0.02% rhamnose for 15-18 h at 37°C and then for 24 h at 18°C. Proteins were purified using Ni-NTA agarose (Qiagen) according to the manufacturer's protocol with minor modification. In wash buffer 400 mM imidazole was substituted with 100 mM EDTA. Fluorescence spectra were recorded using a FluoroMax-3 spectrofluorometer (Jobin Yvon). A Hitachi U-2000 spectrophotometer was used for absorbance measurements.

Extinction coefficient was calculated based on a comparison of absorbance values at the main peak with the absorbance value at the smaller peak at around 390 nm, assuming the latter had extinction coefficient of free BV of 39,900 $M^{-1}cm^{-1}$. To determine quantum yield, fluorescence signal of a purified protein was compared to that of an equally absorbing Nile Blue dye. pH titrations were done using a series of buffers (100 mM sodium acetate, 300 mM NaCl for pH 2.5–5.0 and 100 mM NaH_2PO_4, 300 mM NaCl for pH 4.5–9.0).

To study protein folding and maturation in cells[21], LMG194 bacterial cells were grown at 37°C overnight in RM medium. The next morning, 0.2% rhamnose was added for 2 h, then 0.002% arabinose was added, and cells were cultured for 1 h. Then arabinose was washed out and cells were cultured in RM medium with 0.2% rhamnose at 37°C. Over time fluorescence intensities of the equal aliquots of the cell suspension were measured after dilution to the same optical density of 0.2, and the obtained values were multiplied by the dilution factor. For EGFP expression, the procedure was the same except that LMG194 strain did not contain pWA21h plasmid for heme oxygenase expression.

Protein imaging in phantom mouse

Recombinant far-red GFP-like FPs were expressed in LMG194 bacterial cells and then purified using the Ni-NTA agarose (Qiagen). The purified FPs were diluted to the equal concentrations of 8 μM, calculated based on the extinction coefficients at the chromophore absorbance maxima. The 5 μl volume of each FP was placed 15 mm deep inside into one of two available bores in a XFM-2 phantom mouse (PerkinElmer/Caliper). The bores were located at 7.0 mm and 18.1 mm distance from the imaging surface. Images were taken in 19 different combinations of the far-red and infra-red excitation and emission channels using an epifluorescence mode of the IVIS Spectrum (PerkinElmer/Caliper). A signal-to-background ratio was calculated for each wavelength combination for each FP, using the phantom mouse without protein sample inside as a background reference. All quantitative measurements of fluorescence signal were performed utilizing the Living Image v. 4.3.1 software (PerkinElmer/Caliper). To remove cross bleed form the excitation light an adaptive background subtraction was performed.

Mammalian plasmids and cell culture

The plasmids used for expression of all FPs in mammalian cells were based on pEGFP-N1 backbone (Clontech). To construct the plasmids (piRFP670-N1, piRFP682-N1, piRFP702-N1, piRFP713-N1, piRFP720-N1, pmNeptune-N1, pE2-Crimson-N1, peqFP650-N1, peqFP670-N1) the respective genes were PCR amplified as AgeI-NotI fragments and swapped with a gene of EGFP in pEGFP-N1.

To construct pMito-iRFP670, pMito-iRFP713, and pMito-iRFP720 iRFP670, iRFP713, and iRFP720 genes were cut from N1 plasmids and swapped with mTagBFP gene in pMito-mTagBFP[22]. To generate pNLS-iRFP670, pNLS-iRFP713, and pNLS-iRFP720 iRFP670, iRFP713, and iRFP720 genes were cut from piRFPs-N1 plasmids AgeI-NotI fragments and swapped with a gene of ECFP in the pNLS-ECFP plasmid.

HeLa cell lines were grown in DMEM containing 10% FBS, 0.5% penicillin-streptomycin and 2 mM glutamine (Invitrogen). For microscopy cells were cultured in 35 mm glass bottom culture dishes with no. 1 cover glasses (MatTek). MTLn3 rat adenocarcinoma cells were cultured in αMEM medium (Life Technologies) supplied with 5% FBS, 0.5% penicillin-streptomycin, and 2 mM glutamine (Life Technologies). Plasmid transfections were performed using an Effectene reagent (Qiagen) according to the manufacturer's protocol. Stably-expressing cells were selected with 700 mg/ml G418 antibiotic. Sorting of

positive cells was performed using a MoFlo XDP sorter (Beckman Coulter) equipped with a 676 nm Kr laser and a 700 nm LP emission filter.

Imaging and characterization in mammalian cells

Imaging of HeLa cells was performed 48 h after the transfection. HeLa cells were imaged using an Olympus IX81 inverted epifluorescence microscope equipped with 200 W Me-Ha arc lamp (Lumen220Pro, standardly equipped with 800 nm cold mirror; Prior), 100x 1.4 NA oil immersion objective lens (UPlanSApo, Olympus), and far-red (605/40 nm exciter and 640 nm LP emitter) or Cy5.5 filter sets (665/45 nm exciter and 725/50 nm emitter) (Chroma). Two-color imaging of cells co-transfected with iRFP670 and iRFP720 or iRFP670 and iRFP713 was performed with two filter sets (605/40 nm exciter, 667/30 nm emitter) and (682/12 nm exciter, 721/42 nm emitter). All filter sets were from Chroma. SlideBook v. 4.1 software (Intelligent Imaging Innovations) was used to operate Olympus IX81 inverted microscope.

Spectral imaging of mixtures of MTLn3 cells stably expressing iRFP670, iRFP682, iRFP702, and iRFP720 was performed using Leica TCS SP5 confocal microscope (Leica Microsystems). A 63x 1.4 NA oil immersion objective lens and a 633 nm laser line were used. Emission spectra were detected from 660 nm to 790 nm. The LAS-AF software (Leica Microsystems) was used to operate the microscope and unmix the channels. Spectra of purified FPs were used as references for unmixing. Unmixed channels were pseudocolored and overlaid using ImageJ software (NIH).

Photobleaching experiments were performed in HeLa cells transiently expressing FPs using the Olympus IX81 microscope described above. Raw data were normalized to absorbance spectra and extinction coefficients of the proteins, spectrum of 200 W Me-Ha arc lamp and transmission of 665/45 nm photobleaching filter.

For flow cytometry analysis of effective brightness in mammalian HeLa cells, the piRFP-N1 plasmids coding for FPs were co-transfected with pEGFP-N1 to normalize for transfection efficiency. Fluorescence intensity of cells was analyzed using a either LSRII cytometer (BD Biosciences) equipped with 488 nm and 635 nm lasers and utilizing 530/30 nm, 660/20 nm, 710/20 nm, and 780/60 nm filters or the similar LSRII cytometer (BD Biosciences) equipped with 488 nm and 640 lasers and utilizing 525/30 nm, 670/30 nm, 730/45 nm, and 780/60 nm filters. To quantify cell fluorescence, a mean fluorescent intensity of the non-negative population in the near infra-red channel was divided by a mean fluorescent intensity of the same population in the green channel, thus, normalizing the near-infrared signal to the transfection efficiency. All FACS calculations were performed using FlowJo software (Tree Star).

Cytotoxicity was estimated as a stability of fluorescence over cell generations as described before[13]. MTLn3 cells were transfected with plasmids encoding iRFP670, iRFP682, iRFP702, iRFP713, iRFP720, and EGFP. After several days G418 drug was added to the final concentration of 700 μg/ml to select for stable preclonal mixtures. On day 14 post transfection the cells were sorted using the MoFlo XDP cell sorter, and the brightest fluorescent population for each protein was collected. An aliquot of collected cells were

analyzed the same day using the LSRII cytometer (10,000 events). After 15 more days of culturing in the presence of G418 (29 days after transfection in total) the cells were analyzed using the LSRII cytometer in the same conditions. Histograms representing cell populations and mean fluorescence intensities of the sorted cells were calculated using FlowJo software.

Discrimination of four types of MTLn3 cells stably expressing iRFP670, iRFP682, iRFP702, and iRFP720 (single FP type per cell) was performed using the LSRII cytometer using the 635 nm laser and 660/20 nm and 780/60 nm emission filters. 10,000 events for each cell type were analyzed under the same conditions in one experiment. The obtained dot plots were superimposed.

Construction of adenoviral vectors

The adenovirus serotype V based particles[23] containing the iRFP were obtained using an AdEasy XL Adenoviral Vector System (Stratagene), as described[13].

In vivo imaging

To implant xenograph tumors, 10^6 of MTLn3 cells stably expressing iRFP670, iRFP682, iRFP702, iRFP713, iRFP720, or EGFP (single FP type per cell) were injected into the mammary gland of SCID/NCr mice (female, 5-7 weeks old) (Taconic), and imaged starting 1 week later using the IVIS Spectrum in epifluorescence mode. All mice were imaged in 19 filter channels using the IVIS Spectrum. Belly fur was removed using a depilatory cream. Mice were fed with AIN-93M Maintenance Purified Diet (TestDiet) to reduce intrinsic autofluorescence level. All quantitative measurements of fluorescence signal were made with the Living Image v. 4.3.1.

For fluorescence time course measurement, mice with a single tumor were imaged for four weeks after cell injection. Background-subtracted images of total radiant efficiencies of the same region over tumors were calculated. Filter channels used for calculation of tumor growth curves were the following: 640/30 nm exciter and 680/20 nm emitter for iRFP670, 675/30 nm exciter and 720/20 nm emitter for iRFP682, iRFP702, iRFP713, and 710/30 nm exciter and 710/760 nm emitter for iRFP720.

For two-color imaging of two tumors, mice were injected with MTLn3 cells expressing either iRFP670 or iRFP720 in close sites the same day or with a time difference of one week. For two-color imaging of iRFP670 expressing tumor and iRFP713 expressing liver, mice with xenograph tumor expressing iRFP670 were intravenously injected with 2×10^9 infectious units of an adenovirus at day 18 or 24 day after MTLn3 cell injection.

For spectral imaging of five FPs, mice were injected with two types of MTLn3 cells each the same day. For spectral unmixing, an image cube was collected on the IVIS Spectrum with 19 filter channels. Fluorescence regions were identified and spectrally unmixed using a Living Image v. 4.3.1. Spectral data obtained for individual bacterial streaks expressing iRFP670, iRFP682, iRFP702, iRFP713, or iRFP720 were used as references for unmixing.

For fluorescence imaging tomography (FLIT), mice were depilated and images were taken in transillumination mode. Data acquisition and processing were performed according to the

Living Image v. 4.3.1 protocol. Two fluorescent samples were imaged with different filter sets (640/30 nm exciter and 680/20 nm emitter for iRFP670, 710/30 nm exciter and 710/60 nm emitter for iRFP713), and then overlaid.

The tumors and livers were excised postmortem and imaged using the IVIS Spectrum. All animal experiments were performed in an AAALAC approved facility using protocols approved by the Albert Einstein College of Medicine Animal Usage Committee.

Supplementary Material

Refer to Web version on PubMed Central for supplementary material.

Acknowledgments

We thank E. Giraud (Institute for Research and Development, France) for the *hmuO* and *Rp*BphP6 genes, F. Subach (currently at National Research Center Kurchatov Institute, Russia) for the pWA23h plasmid, G. Filonov (currently at Weill Cornell Medical College) for the iRFP713 adenovirus, J. Zhang for the cell sorting, Y. Wang, L.-M. Ting, X. Wang, and K. Piatkevich for the help with mice, B. Taylor (PerkinElmer/Caliper) for the assistance with the Living Image software, and P. Guo for the help with confocal microscope. This work was supported by grants GM073913, CA164468, and EB013571 from the National Institutes of Health.

References

1. Weissleder R. A clearer vision for in vivo imaging. Nat Biotechnol. 2001; 19:316–317. [PubMed: 11283581]
2. Strack RL, et al. A rapidly maturing far-red derivative of DsRed-Express2 for whole-cell labeling. Biochemistry. 2009; 48:8279–8281. [PubMed: 19658435]
3. Lin MZ, et al. Autofluorescent proteins with excitation in the optical window for intravital imaging in mammals. Chem Biol. 2009; 16:1169–1179. [PubMed: 19942140]
4. Morozova KS, et al. Far-red fluorescent protein excitable with red lasers for flow cytometry and superresolution STED nanoscopy. Biophys J. 2010; 99:L13–15. [PubMed: 20643047]
5. Shcherbo D, et al. Near-infrared fluorescent proteins. Nat Methods. 2010; 7:827–829. [PubMed: 20818379]
6. Subach OM, et al. A photoswitchable orange-to-far-red fluorescent protein, PSmOrange. Nat Methods. 2011; 8:771–777. [PubMed: 21804536]
7. Piatkevich KD, Subach FV, Verkhusha VV. Engineering of bacterial phytochromes for near-infrared imaging, sensing, and light-control in mammals. Chem Soc Rev. 2013; 42:3441–3452. [PubMed: 23361376]
8. Giraud E, Vermeglio A. Bacteriophytochromes in anoxygenic photosynthetic bacteria. Photosynth Res. 2008; 97:141–153. [PubMed: 18612842]
9. Auldridge ME, Forest KT. Bacterial phytochromes: more than meets the light. Crit Rev Biochem Mol Biol. 2011; 46:67–88. [PubMed: 21250783]
10. Giraud E, et al. A new type of bacteriophytochrome acts in tandem with a classical bacteriophytochrome to control the antennae synthesis in Rhodopseudomonas palustris. J Biol Chem. 2005; 280:32389–32397. [PubMed: 16009707]
11. Shu X, et al. Mammalian expression of infrared fluorescent proteins engineered from a bacterial phytochrome. Science. 2009; 324:804–807. [PubMed: 19423828]
12. Auldridge ME, Satyshur KA, Anstrom DM, Forest KT. Structure-guided engineering enhances a phytochrome-based infrared fluorescent protein. J Biol Chem. 2012; 287:7000–7009. [PubMed: 22210774]
13. Filonov GS, et al. Bright and stable near-infrared fluorescent protein for in vivo imaging. Nat Biotechnol. 2011; 29:757–761. [PubMed: 21765402]

14. Filonov GS, et al. Deep-tissue photoacoustic tomography of a genetically encoded near-infrared fluorescent probe. Angew Chem Int Ed Engl. 2012; 51:1448–1451. [PubMed: 22213541]
15. Wagner JR, Brunzelle JS, Forest KT, Vierstra RD. A light-sensing knot revealed by the structure of the chromophore-binding domain of phytochrome. Nature. 2005; 438:325–331. [PubMed: 16292304]
16. Toh KC, Stojkovic EA, van Stokkum IH, Moffat K, Kennis JT. Fluorescence quantum yield and photochemistry of bacteriophytochrome constructs. Phys Chem Chem Phys. 2011; 13:11985–11997. [PubMed: 21611667]
17. Strack RL, et al. A noncytotoxic DsRed variant for whole-cell labeling. Nat Methods. 2008; 5:955–957. [PubMed: 18953349]
18. Ho SN, Hunt HD, Horton RM, Pullen JK, Pease LR. Site-directed mutagenesis by overlap extension using the polymerase chain reaction. Gene. 1989; 77:51–59. [PubMed: 2744487]
19. Wegerer A, Sun T, Altenbuchner J. Optimization of an E. coli L-rhamnose-inducible expression vector: test of various genetic module combinations. BMC Biotechnol. 2008; 8:2. [PubMed: 18194555]
20. Giraud E, et al. Bacteriophytochrome and regulation of the synthesis of the photosynthetic apparatus in Rhodopseudomonas palustris: pitfalls of using laboratory strains. Photochem Photobiol Sci. 2004; 3:587–591. [PubMed: 15170489]
21. Kremers GJ, Goedhart J, van den Heuvel DJ, Gerritsen HC, Gadella TW Jr. Improved green and blue fluorescent proteins for expression in bacteria and mammalian cells. Biochemistry. 2007; 46:3775–3783. [PubMed: 17323929]
22. Subach OM, et al. Conversion of red fluorescent protein into a bright blue probe. Chem Biol. 2008; 15:1116–1124. [PubMed: 18940671]
23. Waddington SN, et al. Adenovirus serotype 5 hexon mediates liver gene transfer. Cell. 2008; 132:397–409. [PubMed: 18267072]

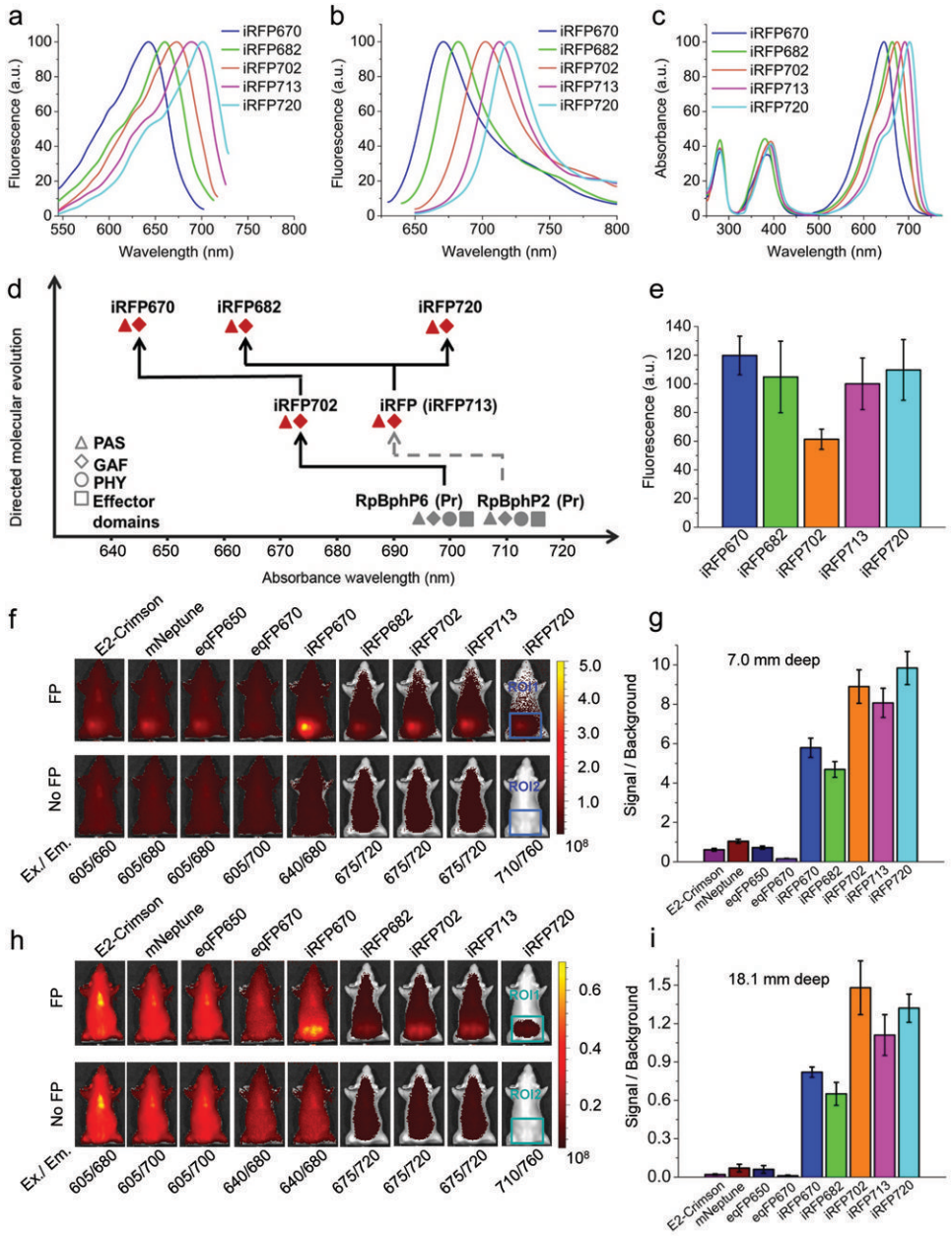

Figure 1. Characterization of NIR FPs

(**a,b**) Normalized excitation (a) and emission (b) spectra of different iRFPs. (**c**) Normalized full absorbance spectra of iRFPs. (**d**) Schematic representation of directed molecular evolution that led to iRFPs with distinct spectral properties. Development of previously reported iRFP713 is shown in a dash line. (**e**) Brightness of HeLa cells transiently transfected with iRFPs, normalized to the value for iRFP713-expressing cells. For each type of cells, the mean NIR fluorescence intensity of cellular population was normalized to FP transfection efficiency (co-transfection with EGFP), excitation efficiency of each FP with the 635 nm laser, and fluorescence signal of each FP in the emission filter Error bars, s.d. (*n* = 3 transfection experiments). (**f**) Comparison of iRFPs with GFP-like far-red FPs as fluorescent probes in deep-tissue imaging. Equal amounts of purified FPs (upper row, FP) or

buffer with no FPs (lower row, no FP) were imaged in epifluorescent mode inside a mouse phantom at 7.0 mm depth using several filter channels. Total radiant efficiencies of the indicated area with the FP sample (ROI1) and without (ROI2) were measured and signal-to-background ratios (ROI1-ROI2)/ROI2 were calculated for each channel. Images with the highest ratio among channels are shown for each FP. The color bar indicates the total fluorescence radiant efficiency ([photon/s/cm^2/steradian]/[μW/cm^2]). (**g**) Quantification of the signal-to-background ratios for the images shown in (f). (**h,i**) Same as in (f,g) with protein samples located at 18.1 mm depth. Error bars, s.d. (n = 4 (g,i)).

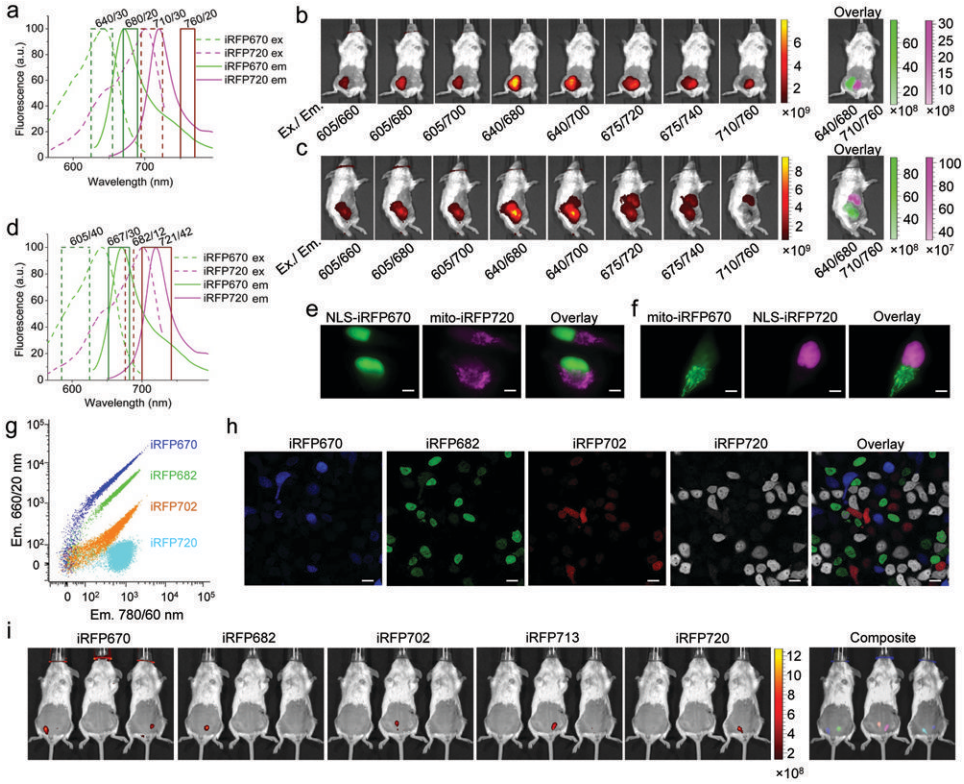

Figure 2. Multicolor imaging *in vivo* and in cells

(a-f) Two-color imaging. (a) Spectra of iRFP670 and iRFP720 were overlaid with the profiles of filter channels optimal for two-color imaging: 640/30 nm excitation and 680/20 nm emission, and 710/30 nm excitation and 760/20 nm emission. (b) Representative images of a living mouse with two co-injected tumors expressing iRFP670 (left tumor) and iRFP720 (right tumor). The images in different channels and the overlay of two optimal channels were obtained on day 24 after cell injections. (c) Representative images of a living mouse with a tumor expressing iRFP670 (lower left) and liver expressing iRFP713 (upper right). The images in different channels and the overlay of two optimal channels were obtained on day 29 after cell injection and day 6 after adenovirus infection. (c,d) The color bars indicate the fluorescent radiant efficiency ([photon/s/cm^2/steradian]/[μW/cm^2]). (d) Spectra of iRFP670 were overlaid with the profiles of the filter channels used in microscopy: 605/40 nm excitation and 667/30 nm emission for iRFP670, and 682/12 nm excitation and 721/42 nm emission for iRFP720. (e,f) Two-color microscopy of transiently transfected HeLa cells co-expressing iRFP670 and iRFP720 in nucleus and mitochondria. The overlays of two pseudocolor images, corresponding to iRFP670 channel (in green, left column) and iRFP720 channel (in magenta, middle column) are shown. Scale bar, 10 μm. **(g-i)** Multicolor spectral imaging. (g) Flow cytometry analysis of MTLn3 cells stably expressing iRFP670, iRFP682, iRFP702, and iRFP720. 10,000 events of each cell type were collected. A 635 nm excitation laser and a combination of two indicated emission filters were used. (h) Confocal microscopy with spectral detection and linear unmixing of four types of MTLn3 cells shown in (g). Emission spectra were detected from 660 nm to 790 nm with an excitation by 633 nm laser. Unmixed channels and the overlay are shown in pseudocolors. Scale bar, 20 μm. (i)

Separate detection of five types of tumors expressing iRFPs in living mice. Mice were injected with two types of MTLn3 cells each, from left to right in each image: iRFP670, iRFP682, iRFP702, iRFP713, iRFP720, and iRFP670. Images were acquired in 19 spectral channels on day 12 after cell injections, and unmixed using reference spectra. Representative images of mice in unmixed channels and the composite pseudocolored image are shown. The color bar indicates the fluorescent radiant efficiency ([photon/s/cm^2/steradian]/[μW/cm^2]).

Table 1

Properties of BphP-derived NIR FPs that were used for *in vivo* imaging.

NIR FP	BphP template	Ex, nm	Em, nm	Extinction coefficient, $M^{-1}cm^{-1}$	Quantum yield, %	Molecular brightness *vs.* iRFP, %	Photostability, $t_{1/2}$, s	p*Ka*	Brightness in HeLa cells *vs.* iRFP, %
IFP1.4	*Dr*BphP	684	708	102,000	7.0	116	70	4.6	8
iRFP670	*Rp*BphP6	643	670	114,000	11.1	205	290	4.0	119
iRFP682	*Rp*BphP2	663	682	90,000	11.3	165	490	4.5	105
iRFP702	*Rp*BphP6	673	702	93,000	8.2	124	630	4.5	61
iRFP713 (formerly iRFP)	*Rp*BphP2	690	713	98,000	6.3	100	960	4.5	100
iRFP720	*Rp*BphP2	702	720	96,000	6.0	93	490	4.5	110